Using AMPERE Data to Understand and Verify Dayside Neutral Wind

Yining Shi[1], Delores Knipp[1], Liam Kilcommons[1], Tomoko Matsuo[2], Brian Anderson[3]
[1]CU Aerospace Engineering Sciences (ASEN), [2]CU CIRES, [2]JH Applied Physics Laboratory (APL)

Abstract

We study a geomagnetic quiet time period on June 14, 2011 using magnetic potential patterns and field-aligned currents (FAC) developed from Active Magnetosphere and Planetary Electrodynamics Response Experiment (AMPERE) data.

On that date, the High-latitude Interferometer Wind Observation (HIWIND) balloon interferometer, indicated equatorward neutral winds on dayside high-latitude region when thermosphere models expected poleward winds during this time period (Wu et al., 2012). Studies by Moe and Wu (2014) and Sheng et al. (2015) reported that unrealistically large dayside heating would be needed to turn the winds to agree with the models.

Zhang et al. (submitted to GRL, 2016) show how the wind reversal can be achieved without the need for extraordinary energy inputs. We provide independent verification of that result by assimilating space-based magnetometer data in the new AMIENext procedure (Matsuo et al, 2015). We generate empirical orthogonal functions (EOFs) from the data to describe the primary modes of variability in magnetic potential. AMIENext result shows the influence of lobe merging/convection related to B_x-,B_y+, and B_z+ IMF configuration.

Background

The HIWIND balloon flying at ~ 68Nº on June 14, 2011 measured equatorward neutral winds in the dayside high-latitude region. However, modeling results for the same time period from Thermosphere Ionosphere Electrodynamics Global Circulation Model (TIEGCM) showed that dayside neutral wind should be poleward (Wu et al., 2012).

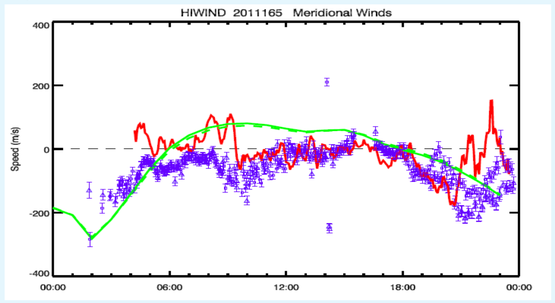

Figure 1: HIWIND, TIEGEM winds and EISCAT ion drifts

Figure 1 shows HIWIND measurements with error bars (blue), TIEGCM results (green) and EISCAT ion drifts (red).

Previous Work

The discrepancy in wind direction mentioned above has been investigated in earlier studies.

- In the work of Moe and Wu (2014), they used a thermospheric model that accounts fore energetic particle precipitation through the magnetosphere cusp during geomagnetic quiet times and increased dayside cusp region density.
- A study by Sheng et al. (2015) also addressed this problem using GITM. They compared the neutral wind results with and without an additional Poynting flux of 75 mW/m^2 and 2 mW/m^2 of 100 eV soft electron precipitation added to a cusp region.

Figure 2 shows the results from Sheng et al. (2015). Additional cusp energy produced an equatorward neutral wind as shown. However, the additional energy was much higher than the background (Poynting flux of 20 mW/m^2 and 1 mW/m^2 of 150 eV electron), it is believed to be unpractical under quiet condition like in this event.

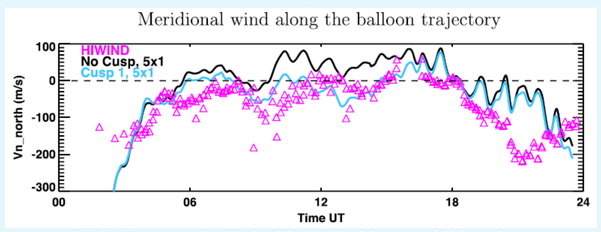

Figure 2: HIWIND, neutral wind with and without additional cusp energy

Data Source - Magnetic Perturbations from AMPERE

Active **M**agnetosphere and **P**lanetary **E**lectrodynamics **R**esponse **E**xperiment (AMPERE) provides magnetic perturbation data with a:

- 20-sec cadence in normal operation, 2-sec in high resolution mode.

Only cross-track data are extracted for a time of interest +/-5 min. Figure 3 shows an example of data coverage at 09:40 UT for both hemispheres when the satellites collected data every 2 seconds.

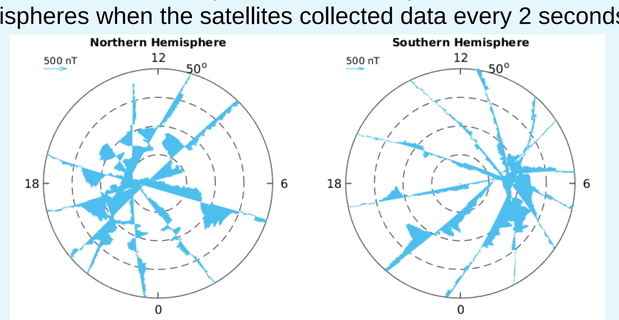

Figure 3: AMPERE magnetic perturbation data at 9:40 UT

Empirical Orthogonal Function (EOF) Analysis

AMPERE data are analyzed using EOF analysis in this study to

- characterize dominant modes of magnetic potential variability and
- subsequently used as input of AMIENext to produce magnetic potential patterns.

A set of EOFs can be used to explain the variability in a magnetic perturbation data set (Matsuo et al., 2002), as

$$\boldsymbol{\delta B}'(\mathbf{r},t) = \boldsymbol{\delta B}(\mathbf{r},t) - \overline{\boldsymbol{\delta B}}(\mathbf{r},t)$$

$$\boldsymbol{\delta B}'(\mathbf{r},t) = \alpha^{(1)}(t)\cdot \mathbf{EOF}^{(1)}(\mathbf{r}) + \alpha^{(2)}(t)\cdot \mathbf{EOF}^{(2)}(\mathbf{r}) + \cdots + \mathbf{e}'(\mathbf{r},t)$$

where the residual of the magnetic is represented by the sum of EOFs weighted by time-dependent coefficients and the residual perturbation not explained by the EOFs. Each EOF is determined by a sequential non-linear regression analysis.

The mean and EOFs of magnetic potential are obtained using magnetic perturbation EOFs and a set of modified spherical cap harmonic basis functions (Richmond and Kamide, 1988).

Figure 4 shows the mean and first three EOFs of magnetic potential obtained using data from June 11 to June 17, 2011 with 10 min resolution for both northern hemisphere (NH) (a) and southern hemisphere (SH) (b).

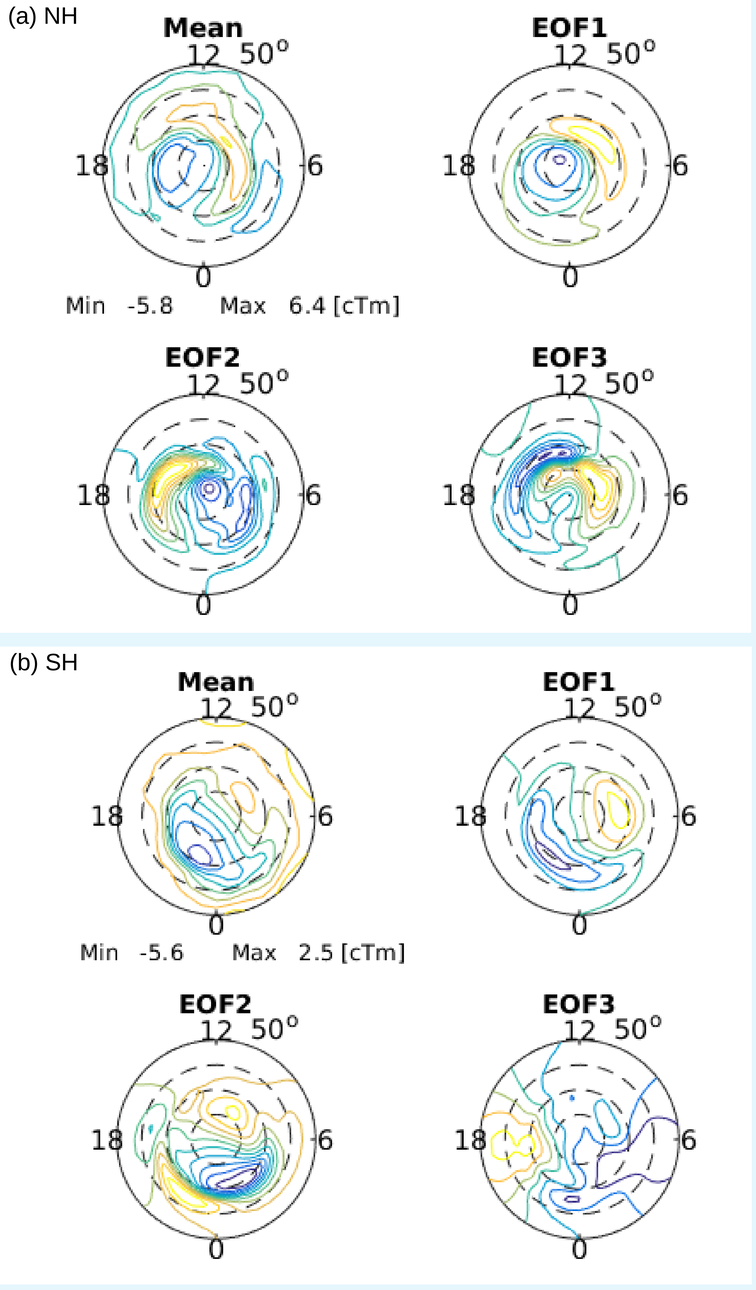

Figure 4: Mean and first three EOFs magnetic potential patterns

The mean and EOFs are plotted in geomagnetic coordinates from 50º to 90º. Red contours are positive and blue ones are negative for the mean pattern. EOFs are normalized between -1 and 1. 32% of variability is explained in these patterns for NH while for SH, only 9% is explained. This indicates that SH is much noisier and changes more randomly with time.

Conclusions

We studied the event on June 14, 2011 where the HIWIND balloon measurement showed unexpected equatorward neutral wind under mostly quiet geomagnetic condition.

First we generated EOFs from a full week of AMPERE magnetic perturbation data to take a look at the dominant modes of variability in magnetic potential. We see that NH is dominated by dayside activity while SH changes more randomly.

Magnetic potential maps are then produced using AMIENext procedure and maps for different IMF configurations are studied. Under B_z- conditions, magnetic potential shows a two cell pattern as expected. When B_z turned persistently northward later along with B_x - and B_y +, we can see the influence of lobe merging/convection on NH dayside.

Ion-neutral coupling in the persistent lobe cell likely produced an equatorward wind in the vicinity of the HIWIND balloon (Zhang et al, 2016, submitted to GRL). **Our patterns confirm those of Zhang et al., determined from MHD modeling and polar orbiting ion drift measurements**

With the 5 min resolution we have in this study, we can also capture short-time variability in magnetic variables.

Assimilative Mapping of Ionospheric Electrodynamics (AMIE)

With the extended AMIENext (Matsuo et al., 2015), we:

- produce magnetic potential maps from AMPERE data using mean and EOFs and
- use magnetic potential to invert the space-based magnetometer data to obtain field-aligned currents (FACs).

We generated magnetic potential and FACs for June 14, 2011. B_z stayed positive for most of the (Figure 5), giving a geomagnetic quiet day.

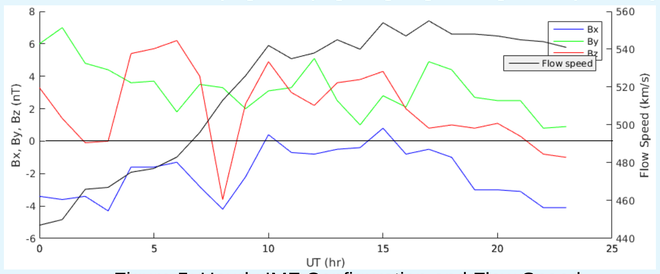

Figure 5: Hourly IMF Configuration and Flow Speed

B_z went to ~ -5 nT around 09 UT on this day, enhancing the magnetic potential for both hemispheres and forming patterns normally associated with B_z -conditions. Figure 6 shows the magnetic potential contours for both hemisphere at 09:40 UT as an example.

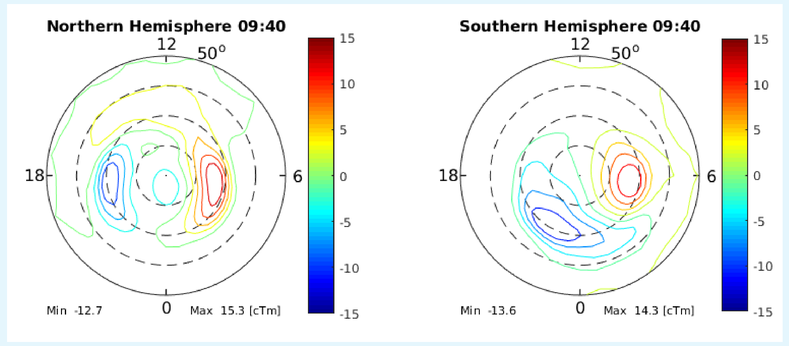

Figure 6: Magnetic Potential Maps at 09:40 UT for Both Hemisphere

The IMF turned to B_x-, B_y+ and B_z+ later for a long period of time. To study the influence of this IMF configuration, the averaged magnetic potential contours and FAC color map for both hemispheres from 12:00 UT to 17:30 UT are shown in Figure 7. We can see the influence of lobe merging/convection on dayside occurring in NH but not SH. The result for NH is consistent with the modeling result from Zhang et al. (2016).

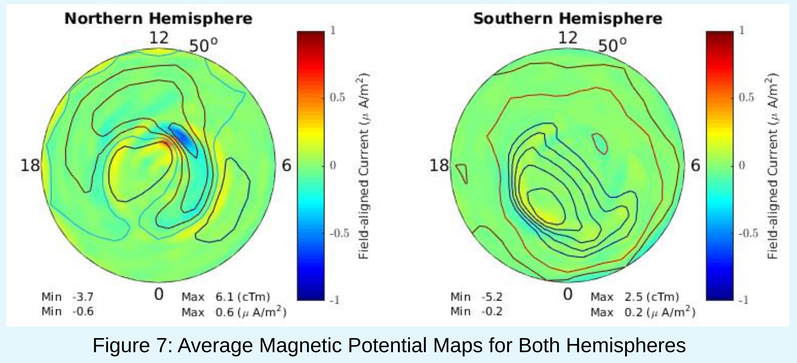

Figure 7: Average Magnetic Potential Maps for Both Hemispheres

In addition to the average maps, we also looked at the variability of magnetic potential with time. Figure 8 provides two examples where magnetic potential patterns show significant deviation from the average. This shows the ability of AMIENext to capture short time changes in electrodynamic variables.

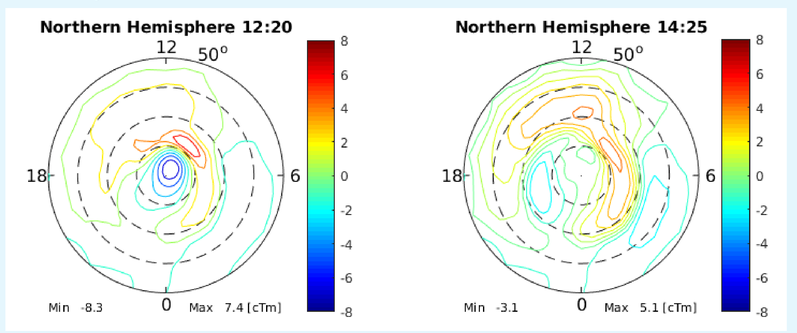

Figure 8: Northern Hemisphere Magnetic Potential Maps at 12:20 UT and 14:25 UT

References And Acknowledgements

We thank the AMPERE team and the AMPERE Science Center for providing the Iridium-derived data products.

Matsuo T, Knipp D J, Richmond A D, et al. Inverse procedure for high-latitude ionospheric electrodynamics: Analysis of satellite-borne magnetometer data[J]. JGR: Space Physics, 2015, 120(6): 5241-5251.

Matsuo, T., Richmond, A. D., & Nychka, D. W. (2002). Modes of high-latitude electric field variability derived from DE-2 measurements: Empirical orthogonal function (EOF) analysis. GRL, 29(7).

Moe K, Wu Q. Impact of HIWIND balloon measurements on thermospheric density models[J]. JGR: Space Physics, 2014, 119(4): 2476-2483.

Sheng C, Deng Y, Wu Q, et al. Thermospheric winds around the cusp region[J]. JGR: Space Physics, 2015, 120(2): 1248-1255.

Wu Q, Wang W, Roble R G, et al. First daytime thermospheric wind observation from a balloon-borne Fabry-Perot interferometer over Kiruna (68N)[J]. GRL, 2012, 39(14).

Richmond A D, Kamide Y. Mapping electrodynamic features of the high-latitude ionosphere from localized observations: Technique[J]. Journal of Geophysical Research: Space Physics, 1988, 93(A6): 5741-5759.

Zhang B et al. Effects of magnetospheric lobe-cell convection on dayside upper thermospheric winds at high-latitudes, submitted to GRL, 2016